Ionization fronts in planar dc discharge systems with high-ohmic electrode

Sh. Amiranashvili, S. V. Gurevich, and H.-G. Purwins
Institut für Angewandte Physik, Corrensstr. 2/4, D-48149 Münster, Germany
(Received 19 January 2005; published 20 June 2005)

Electric breakdown and ionization fronts are considered theoretically in a sandwichlike dc discharge system consisting of two plane-parallel electrodes and a gaseous gap in between. The key system feature is a high-ohmic cathode opposite to an ordinary metal anode. Such systems have received much attention from experimental studies because they naturally support current patterns. Using adiabatic description of electrons and two-scale expansion we demonstrate that in the low-current Townsend mode the discharge is governed by a two-component reaction-diffusion system. The latter provides quantitative system description on the macroscopic time scale (i.e., much larger than the ion travel time). The breakdown appears as an instability of the uniform overvoltage state. A seed current fluctuation triggers a shocklike ionization front that propagates along the discharge plane with constant speed (typically $\sim 10^4$ cm/s). Depending on the cathode resistivity the front exhibits either monotonic or oscillatory behavior in space. Other breakdown features, such as damping transient oscillations of the global current, can also be found as solutions of the reaction-diffusion equations.

DOI: 10.1103/PhysRevE.71.066404 PACS number(s): 52.80.Dy, 52.35.Tc, 52.65.−y, 82.40.Ck

I. INTRODUCTION

Self-organized lighting current patterns like striations in long discharge tubes or current spots in laterally extended systems are complicated in nature though relatively easy to generate [1]. Despite the good knowledge of the underlaying microscopic processes, the observed macroscopic patterns (e.g., anode spots) are not understood to large extent. One reason is that typically the current patterns are three-dimensional (3D) objects that evolve on a time scale of a millisecond or longer. In contrast, the smallest time scale that should be taken into account, e.g., in the popular drift-diffusion approximation, is the electron travel time that is of order of 10 nanoseconds for the systems in question. A direct numerical solution of the plasma transport equations is therefore very time consuming or even impossible. The alternative is to develop an appropriate reduced discharge model. In what follows we solve this problem for the Townsend discharge.

A concrete experimental system that we have in mind is the planar dc discharge system in which one metal electrode is separated from the gas by a high-ohmic barrier, as first suggested in Refs. [2–4]. In this case the electric potential is not necessarily constant along the interface of the high ohmic barrier and the gas layer. The position dependence of potential of the gas-electrode interface supports a nonuniform discharge distribution, e.g., current spots or current filaments.

The discharge in systems with high ohmic barrier is similar to a dielectric barrier discharge, as it is greatly affected by surface charges [5] and often supports numerous current filaments instead of a single cathode spot. At the same time it is a dc discharge where the current flows exclusively in one direction. Such systems with high-ohmic cathode have been intensely investigated in the last decade [6–15] and a number of exciting structures were observed and interpreted within a qualitative approach using current tools from the field of nonlinear dynamics and pattern formation [16]. However, so far no quantitative approach has been put forward and there was no basis for comparison to experiment. The present paper is dedicated to this problem.

The geometry of the discharge cell in question is shown in Fig. 1. The gas layer is located parallel to the xy plane and extends from $z=0$ to $z=d$ in z direction. The current is essentially parallel to z axis. The cathode consists of a high-ohmic barrier located at $d<z<d+d_c$. Two planar metal contacts are located at $z=0$ (anode) and $z=d+d_c$. Both d and d_c are considerably smaller than the radius of the discharge cell. Consequently, the x and y dependence of the electric potential and particle densities is assumed to be weak compared with the z dependence. Nevertheless, the radial dependence cannot be ignored completely, as it is responsible for laterally extended pattern we are interested in. Two-scale approach will then be used in what follows [17,18].

We now consider the development of electric breakdown in Townsend mode, and look for peculiarities resulting from the high-ohmic barrier. Let us assume that by proper choice

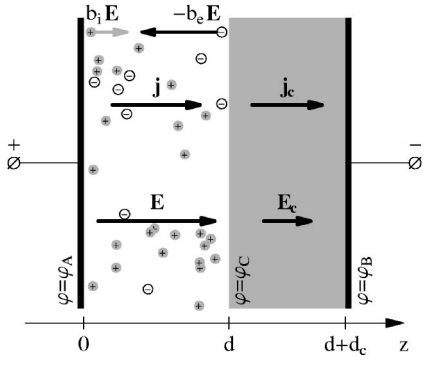

FIG. 1. A cross section of a typical planar discharge cell consisting of a metal anode, a gas layer, a high-ohmic cathode, and another metal contact. $\varphi_A(t)$, $\varphi_C(x,y,t)$, and $\varphi_B(t)$ are potentials at $z=0$, $z=d$, and $z=d+d_c$. $\mathbf{E}$ and $\mathbf{E}_c$ denote the axial electric fields, $\mathbf{j}$ and $\mathbf{j}_c$ are the current densities. Drift velocities of particles are schematically shown at the top. We take nitrogen at $p=1.33\times10^4$ Pa and $d=d_c=0.1$ cm as an example. A typical semiconductor cathode has specific resistivity $\rho\simeq10^7$ Ω cm and dielectric constant $\epsilon\simeq10$.

of the supply voltage the system is prepared to operate near to the breakdown point, that is, the voltage applied to the gas almost equals the Townsend breakdown voltage U_b. In this mode of operation the current is negligible and is often localized in several narrow channels caused by inhomogeneities of the system. The channels serve as seed current fluctuations for the breakdown. The supply voltage is then suddenly increased to a larger value U_s such that

$$U_s - U_b \ll U_b. \tag{1}$$

In this situation parameters of the system, like diffusion and mobility coefficients for electrons and ions, are not changed whereby the ionization coefficient varies considerably due to the strong dependence on the electric field. Note, that in many experiments with the high-ohmic barrier the difference $U_s - U_b$ is several tens of volts, whereas U_b is several hundreds of volts [15,19]. Another example is a direct experimental measurement of U_b, where $U_s - U_b$ can approach one volt [20].

Breakdown in a system like Fig. 1 transfers it to a state that is assumed to be in the Townsend mode. In the case that the current density is uniform, it is determined by

$$j = j_0 = \frac{U_s - U_b}{\rho d_c}, \tag{2}$$

where ρ is the specific resistivity of the high ohmic barrier. The value of j_0 is assumed to be small enough in order to neglect space-charge effects. Typically $j_0 < 10^{-4}$ A/cm^2 if the system is on the right-hand branch of the Paschen curve [1], and $j_0 < 10^{-2}$ A/cm^2 for the left-hand branch [21]. In this way the discharge is operated in the Townsend mode. The breakdown can be considered as a transition between the states with $j=0$ and $j=j_0$. Our goal is to investigate such a transition.

Inequality (1) ensures that the voltage drop $U_{\mathrm{gas}} = \varphi_A - \varphi_C$ at the gas gap is not very different from the breakdown value. Consequently it is natural to present the gap voltage as

$$U_{\mathrm{gas}} = U_b + \delta U(x,y,t), \quad \delta U \ll U_b,$$

where δU is referred to as *the overvoltage*. The essential difference from the familiar case of metal electrodes is that in the case of Fig. 1 both φ_C and δU can depend on position. The maximal possible overvoltage is achieved if the whole supply voltage is applied to the gas gap, i.e.,

$$\delta U(x,y,t) \leqslant U_s - U_b, \tag{3}$$

where the right-hand side is a predetermined quantity, whereas the left-hand side is a dynamical variable to be found.

The major part of the gas electric field $\mathbf{E}$ is directed parallel to the z axis. This axial field component can be presented as

$$E_z = E_b + \delta E, \quad \int_0^d \delta E(x,y,z,t)dz = \delta U, \tag{4}$$

where $E_b = U_b/d$ is the breakdown field. The radial electric field $\mathbf{E}_\perp$ can be exactly calculated at the gas-electrode interfaces

$$\mathbf{E}_\perp\big|_{z=0} = \mathbf{0}, \quad \mathbf{E}_\perp\big|_{z=d} = \boldsymbol{\nabla}_\perp \delta U,$$

where $\boldsymbol{\nabla}_\perp = (\partial_x, \partial_y)$. The first (anode) equation holds for any metal electrode and the second (cathode) follows from the definition of the overvoltage. Due to the small width of the discharge cell, the intrinsic radial field can be approximated as

$$\mathbf{E}_\perp = \frac{z}{d}\boldsymbol{\nabla}_\perp \delta U, \tag{5}$$

the approximation can be also justified by a systematic calculation of the electric field. As ensured by (1) and (3), both axial and radial distortion of E_b are small. As a result the absolute value of the electric field is always approximated as $E_b + \delta E$.

In what follows we derive an equation for the current density in the gas gap. The calculation results in a nonlinear diffusion equation, however, this equation contains δU. For the interplay between the current and the overvoltage we then derive an additional equation considering Laplace equation for the potential and boundary conditions for the electric field. By doing this a closed system of equations for the current density and the overvoltage is obtained. We demonstrate that breakdown occurs in the form of shocklike ionization fronts that we investigate in detail. The results are finally summarized and discussed.

II. THE GAS GAP

In this section we discuss the gas gap where electrons and positively charged particles move in opposite direction as prescribed by the applied electric field. Only one positive charge carrier specie (ions) is considered. The drift velocity of electrons and ions is determined by mobilities $b_{e,i}$,

$$\mathbf{v}_e = -b_e\mathbf{E} \quad \text{and } \mathbf{v}_i = b_i\mathbf{E}.$$

There is also a stochastic particle flux described by the diffusion coefficients $D_{e,i}$. Both mobility and diffusion coefficients depend on the local electric field. However, in the Townsend mode they can be assumed to be constant determined by E_b. The particle densities of electrons n_e and ions n_i are governed by two continuity equations,

$$\partial_t n_{e,i} + \boldsymbol{\nabla}(n_{e,i}\mathbf{v}_{e,i} - D_{e,i}\boldsymbol{\nabla} n_{e,i}) = S_{e,i},$$

where $S_{e,i}$ is the ionization source term. The equations can be rewritten in a simpler form

$$\partial_t n_{e,i} + \mathbf{v}_{e,i}\boldsymbol{\nabla} n_{e,i} - D_{e,i}\boldsymbol{\nabla}^2 n_{e,i} = S_{e,i},$$

as the space-charge effect is negligible in the Townsend mode.

Let us undertake the following simplifications. We use a local field approximation and write

$$S_e = S_i = \alpha(E) n_e v_e,$$

where Townsend parameter $\alpha(E)$ describes ionization rate and $E = E_b + \delta E$. Even if very small, δE should be taken into account here because α is a sharp function of the electric field. Note, that the local field approximation is not a good

model in the case that the electric field is subject to drastic changes, e.g., in the cathode fall. In the Townsend mode, however, the field is practically constant and therefore the simple local ionization term is justified. Farther, the ion diffusion is completely neglected. We also neglect the electron diffusion in the axial direction (see, e.g., Ref. [22]). In contrast to this, the radial diffusion of electrons is taken into account. We also keep the radial drift terms for electrons and ions considering them as a small perturbation with respect to the axial drift flux. Finally, we are interested in processes that are slower than the typical ion travel time

$$\tau_i = \frac{d}{b_i E_b},$$

and consequently $\partial_t n_i$ is taken into account as a small perturbation. The dependence of n_e on time is eliminated adiabatically by setting $\partial_t n_e$ to zero.

Altogether, the continuity equations for electrons and ions are rewritten as

$$[b_e \partial_z n_e + b_e \alpha(E) n_e] E_z = - b_e \mathbf{E}_\perp \boldsymbol{\nabla}_\perp n_e - D_e \boldsymbol{\nabla}_\perp^2 n_e, \quad (6)$$

$$[b_i \partial_z n_i - b_e \alpha(E) n_e] E_z = - b_i \mathbf{E}_\perp \boldsymbol{\nabla}_\perp n_i - \partial_t n_i, \quad (7)$$

where $\boldsymbol{\nabla}_\perp^2$ is the radial part of the Laplace operator. The left-hand sides of Eqs. (6) and (7) provides us with the classical (Townsend) discharge solution; the right-hand side describes its perturbation due to radial drift, radial electron diffusion, and ion inertia.

Of course, appropriate boundary conditions must be imposed on the electrodes. In this context we remember that the diffusion in the axial direction is completely ignored, i.e., the boundary conditions can be taken in the Townsend form [1]

$$n_i|_{z=0} = 0 \quad \text{and} \quad \left.\frac{n_e}{n_i}\right|_{z=d} = \gamma \frac{b_i}{b_e}, \quad (8)$$

where the secondary emission coefficient γ is the ratio of the secondary electron flux from the cathode and the primary ion flux to the cathode.

A. Townsend solution

Our first concern is to reproduce the classical solution for the Townsend discharge [1]. To this end we ignore the right-hand sides of Eqs. (6) and (7) and replace E by the electric breakdown field E_b. The expressions for the electron and ion densities are

$$n_e = e^{-\alpha_b z} n_0, \quad (9)$$

$$n_i = \frac{b_e}{b_i}(1 - e^{-\alpha_b z}) n_0, \quad (10)$$

where $\alpha_b = \alpha(E_b)$. The well-known additional restriction

$$\gamma(e^{\alpha_b d} - 1) = 1 \quad (11)$$

results from the cathode boundary condition and implicitly determines E_b. The parameter n_0 is a constant of integration and can be interpreted as the electron density at the anode; n_0 depends on all space-time variables but z, this dependence is assumed to be slow on the time scale τ_i and space scale d. The electric current density is approximated as

$$j = q b_e E_b n_0, \quad (12)$$

is parallel to the z axis, and depends on all variables but z. In (12) q is the elementary charge.

It is appropriate to assume that n_0 is the true anode electron density, so that a possible distortion of (9) disappears at $z=0$. A possible distortion of (10) disappears at the anode as well, because of the anode boundary condition (8). In what follows a dynamical equation for $n_0(x,y,t)$ will be found as a compatibility condition of the next step of the perturbation expansion. It will then be transformed to a more physical equation for the axial current, as given by (12).

B. The perturbation of the Townsend solution

If one takes the right-hand sides of Eqs. (6) and (7) into account, Eqs. (9) and (10) are not exact solutions. Therefore we perform the next step of the perturbation theory and write the particle densities as follows:

$$n_e = e^{-\alpha_b z} n_0 + \delta n_e,$$

$$n_i = \frac{b_e}{b_i}(1 - e^{-\alpha_b z}) n_0 + \delta n_i,$$

where the perturbations $\delta n_{e,i}$ originate from the radial drift, electron diffusion, and ion inertia. These densities must be substituted into Eqs. (6) and (7). As explained above, we can assume $\delta n_{e,i} = 0$ at $z=0$, but not at $z=d$. A compatibility condition for the resulting equations set is a desired dynamical equation for n_0.

It is profitable to rewrite $n_{e,i}$ in the equivalent form that is suggested by the structure of the Townsend solution. Without loss of generality we introduce $\tilde{n}_{e,i}$ instead of $\delta n_{e,i}$ so that

$$n_e = e^{-\alpha_b z}(n_0 + \tilde{n}_e), \quad (13)$$

$$n_i = \frac{b_e}{b_i}(1 - e^{-\alpha_b z})(n_0 + \tilde{n}_e) + \tilde{n}_i, \quad (14)$$

where $\tilde{n}_{e,i} = 0$ at $z=0$. The variable $\tilde{n}_e$ describes the distortion of n_0 whereas $\tilde{n}_i$ is a "non-Townsend" part of the perturbation. Equation (13) and the electric field (4) and (5) are now inserted into (6). Omitting high-order terms we arrive at the equation for the perturbed electron density

$$\partial_z \tilde{n}_e = - z \boldsymbol{\nabla}_\perp n_0 \boldsymbol{\nabla}_\perp \frac{\delta U}{U_b} - \lambda_e \boldsymbol{\nabla}_\perp^2 n_0 - \alpha_b' n_0 \delta E, \quad (15)$$

where $\alpha_b' = \alpha'(E_b)$ comes from the Taylor expansion of the ionization coefficient. The parameter

$$\lambda_e = \frac{D_e}{b_e E_b}$$

is recognized as the electron diffusion length. We now integrate (15) from $z=0$ to $z=d$ and arrive at the equation

$$\tilde{n}_e|_{z=d} = -\frac{d^2}{2}\nabla_\perp n_0 \nabla_\perp \frac{\delta U}{U_b} - \lambda_e d\nabla_\perp^2 n_0 - \alpha_b' n_0 \delta U, \quad (16)$$

which together with (13) determines δn_e at the cathode.

In a similar manner we substitute (14) into (7) to get the following equation for $\tilde{n}_i$:

$$\frac{b_i}{b_e}\partial_z \tilde{n}_i = (1 - e^{-\alpha_b z})\left(\lambda_e \nabla_\perp^2 n_0 - \frac{\tau_i}{d}\partial_t n_0\right) + \alpha_b' n_0 \delta E.$$

Integration over $0 < z < d$ gives the result

$$\frac{b_i}{b_e}\tilde{n}_i\bigg|_{z=d} = \left(1 - \frac{1 - e^{-\alpha_b d}}{\alpha_b d}\right)(\lambda_e d\nabla_\perp^2 n_0 - \tau_i \partial_t n_0) + \alpha_b' n_0 \delta U \quad (17)$$

together with Eqs. (14) and (16) determining δn_i at the cathode. Note, that both δn_e and δn_i contain $\nabla_\perp \delta U$; the term is specific for our problem and disappears for the metal electrodes.

C. Governing equation

The axial electric field, as given by (4), contains the unknown perturbation δE. That is the reason for deriving equations only for the $\tilde{n}_{e,i}$ at $z=d$. This information is however sufficient to determine n_0. We substitute (13) and (14) in the cathode boundary condition (8) to get $\tilde{n}_i|_{z=d}=0$, i.e., the "non-Townsend" part $\tilde{n}_i$ must disappear at the cathode. Equation (17) reduces to the compatibility condition

$$\tau_i \partial_t n_0 = \lambda_e d\nabla_\perp^2 n_0 + C_\gamma \alpha_b' n_0 \delta U, \quad (18)$$

which is the desired equation for n_0. The familiar inequality $\gamma \ll 1$ was not used in the derivation, nevertheless the numerical factor

$$C_\gamma = \frac{1+\gamma}{1 - \ln^{-1}(1 + 1/\gamma) + \gamma}$$

is of order unity for all reasonable γ. Equation (18) is not closed, as it contains δU. It is of interest to note that the terms containing $\nabla_\perp \delta U$ cancel so that Eq. (18) is formally similar to that for the metal electrodes [23–25], where the overvoltage is compensated by diffusion and the radial drift flux is not important. The difference is that in our work δU is a dynamical variable in a *partial* differential equation to be derived from the consideration of the high-ohmic barrier. Before doing so let us discuss (18) in more details. It is a nonlinear diffusion equation, the corresponding diffusion parameter

$$D_a = \frac{\lambda_e d}{\tau_i} = D_e \frac{b_i}{b_e}$$

is recognized as the ambipolar diffusion coefficient. This fact is not unexpected [26,27] because the spatial spreading of particles is due to electron diffusion, whereas the typical microscopic time scale for the current is determined by the ion travel time. Equation (18) has two uniform stationary solutions either with $n_0=0$ (zero current) or with $\delta U=0$ and n_0 =const, the latter results from the equilibration of j [Eq. (12)] and j_0 [Eq. (2)].

To account for the nonlinearity term let us introduce a multiplication coefficient

$$\mu = \gamma\left[\exp\left(\int_0^d \alpha(E)dz\right) - 1\right]$$

so that $j(t+\tau_i) \approx \mu j(t)$ in accordance with the physical sense of $\alpha(E)$ (see, e.g., Ref. [28]). In the case of slow evolution the Taylor expansion yields

$$\tau_i \partial_t j(t) \approx (\mu - 1) j(t), \quad (19)$$

where the self-sustain condition $\mu=1$ is achieved for $E=E_b$ and is equivalent to (11). For small overvoltage the multiplication coefficient is

$$\mu(E_b + \delta E) \approx \gamma(e^{\alpha_b d + \alpha_b' \delta U} - 1) \approx 1 + \alpha_b' \delta U$$

and the nonlinear term in (18) is restored from (19) up to factor C_γ.

We stress that (18) is applicable to slow (i.e., $\tau_i \partial_t \ll 1$) processes, correspondingly

$$\alpha_b' \delta U \ll 1 \quad (20)$$

that imposes a restriction on $U_s - U_b$. We use the standard approximation for the Townsend coefficient [1]

$$\alpha(E) = Ape^{-Bp/E},$$

where A and B are gas-dependent parameters, p being the pressure. The value α' takes its maximal value at the inflection point (where $E=\frac{1}{2}Bp$) and quickly decreases with either increase or decrease of the electric field, the maximal value of δU is $U_s - U_b$. Inequality (20) is ensured if

$$U_s - U_b \ll \frac{e^2 B}{4A}, \quad (21)$$

where the right-hand side varies from 20 to 60 volts for different gases. Condition (21) refines our original assumption (1).

Finally we rewrite (18) for the axial electric current density j,

$$\partial_t j = D_a \nabla_\perp^2 j + C_\gamma \frac{\alpha_b' \delta U}{\tau_i} j \quad (22)$$

as determined by (12), and turn to the consideration of the high-ohmic barrier.

III. THE HIGH-OHMIC BARRIER

In this section we derive the missing equation for the overvoltage $\delta U(x,y,t)$, which will turn out to be a linear partial differential equation. To begin with we note that the combination $\epsilon_0 \epsilon \partial_t E_z + j_z$ must be continuous at the gas-cathode interface so that

$$(\epsilon_0 \partial_t E_z + j)_{z=d-0} = (\epsilon_0 \epsilon \partial_t E_z + j_c)_{z=d+0}, \quad (23)$$

where the Townsend approximation for the axial electric current density j in the gas is given by (12), j_c is the axial current density in the cathode, and ϵ is the cathode dielectric

constant. We consider the cathode as a simple linear conductor with the specific resistivity ρ, so that $j_c = E_z/\rho$. Now, the problem is reduced to the calculation of the axial electric field E_z. For the special case of spatially uniform $\delta U(t)$ the field equals $(U_b + \delta U)/d$ in the gas and $(U_s - U_b - \delta U)/d_c$ in the cathode. Inserting both fields in (23) we arrive at the standard approximation [25]

$$\mathfrak{c}\partial_t \delta U = \frac{U_s - U_b - \delta U}{\rho d_c} - j, \tag{24}$$

where the combination

$$\mathfrak{c} = \frac{\epsilon_0}{d} + \frac{\epsilon_0 \epsilon}{d_c} \tag{25}$$

is the cell capacity per unit area. It is also profitable to introduce characteristic cathode time

$$\tau_c = \rho d_c \mathfrak{c},$$

which is recognized as the *RC* time of the corresponding circuit. The last term in Eq. (25) usually dominates, τ_c reduces then to $\epsilon_0 \epsilon \rho$, i.e., to the Maxwell time of cathode material. The interplay of τ_c and the ion travel time τ_i plays an important role in what follows.

Equation (24) is only the first approximation to the final equation for the overvoltage because the nonuniformity of δU was completely ignored. To take this nonuniformity into account we need an accurate solution of the Laplace equation with the corresponding boundary conditions. It can be given explicitly due to the small width of the discharge cell. Let us start with the gas region.

Note, that the electric potential at the metal contacts φ_A at $z=0$ and φ_B at $z=d+d_c$ (see Fig. 1) can depend only on time, the difference $U_s = \varphi_A - \varphi_B$ is fixed and equal to the supply voltage. On the contrary, the potential φ_C at the gas-cathode interface at $z=d$ depends on all variables, but z. To get the electric field in gas we must solve the following problem:

$$\boldsymbol{\nabla}^2 \varphi = 0, \quad \varphi\big|_{z=0} = \varphi_A, \quad \varphi\big|_{z=d} = \varphi_C,$$

where the radial part of the Laplace operator is a small perturbation to the axial part. A corresponding solution is obtained as a perturbation expansion in the parameter d/R, where R is the characteristic transversal space scale of the radial structure in question. The electric potential in the gas reads as

$$\varphi = \varphi_A - \frac{z}{d}(\varphi_A - \varphi_C) - \frac{z^3 - z d^2}{6d}\boldsymbol{\nabla}_\perp^2 \varphi_C,$$

where the terms $\sim d^4/R^4$ are ignored. We insert $\varphi_A - \varphi_C = U_b + \delta U$ in the last equation and come to Eq. (5) for the radial electric field, whereas the axial field is given by

$$E_z = \frac{U_b + \delta U}{d} - \frac{3z^2 - d^2}{6d}\boldsymbol{\nabla}_\perp^2 \delta U$$

in accordance with (4), i.e., we have

$$E_z\big|_{z=d-0} = E_b + \frac{\delta U}{d} - \frac{d}{3}\boldsymbol{\nabla}_\perp^2 \delta U$$

for the boundary value of the electric field.

The electric field in the cathode is a solution of a similar problem,

$$\boldsymbol{\nabla}^2 \varphi = 0, \quad \varphi\big|_{z=d} = \varphi_C, \quad \varphi\big|_{z=d+d_c} = \varphi_B,$$

where $\varphi_C - \varphi_B = U_s - U_b - \delta U$. It is easy to demonstrate that

$$E_z\big|_{z=d+0} = \frac{U_s - U_b - \delta U}{d_c} + \frac{d_c}{3}\boldsymbol{\nabla}_\perp^2 \delta U.$$

We finally insert the electric fields in the boundary condition (23), omit small terms, and arrive at

$$\partial_t \delta U = D_c \boldsymbol{\nabla}_\perp^2 \delta U + \frac{U_s - U_b - \delta U}{\tau_c} - \frac{j}{\mathfrak{c}}, \tag{26}$$

which is the desired extension of Eq. (24) for the overvoltage. Formally the combination

$$D_c = \frac{d_c^2}{3\tau_c}$$

can be considered as a diffusion coefficient; the operator $\boldsymbol{\nabla}_\perp^2$ originates however from the radial component of the electric field and does not describe any real diffusion.

Equations (22) and (26) provide a self-consistent description of the physical system depicted in Fig. 1. Their solutions are investigated in the next section.

IV. DISCUSSION OF THE REDUCED SYSTEM

In this section we investigate (22) and (26) and discuss the physical meaning of the corresponding solutions. Let us introduce normalized variables,

$$u = \frac{j}{j_0} \quad \text{and} \quad v = \frac{\delta U}{U_s - U_b},$$

and the dimensionless overvoltage parameter,

$$s = C_\gamma \alpha_b' (U_s - U_b) \ll 1.$$

Parameter s shall be small in accordance with (20). We now rewrite (22) and (26) as a two-component reaction-diffusion system

$$\tau_u \partial_t u = d_u^2 \boldsymbol{\nabla}_\perp^2 u + uv, \tag{27}$$

$$\tau_v \partial_t v = d_v^2 \boldsymbol{\nabla}_\perp^2 v + 1 - u - v. \tag{28}$$

The system is our main result. It is somewhat similar to different qualitative models developed by several authors, but is quantitative, i.e., the characteristic time scales

$$\tau_u = \frac{\tau_i}{s} \quad \text{and} \quad \tau_v = \tau_c,$$

and the diffusion lengths

TABLE I. Typical relaxation times and diffusion lengths for the system (27) and (28). We assumed $\gamma=0.02$ and $U_s-U_b=10$ V, for the other parameters of the discharge cell see Fig. 1.

τ_u	d_u	τ_v	d_v
4.1×10^{-6} s	1.7×10^{-2} cm	9.7×10^{-6} s	5.7×10^{-2} cm

$$d_u=\sqrt{\frac{\lambda_e d}{s}} \quad \text{and} \quad d_v=\frac{d_c}{\sqrt{3}},$$

can be quantitatively calculated for any system in question. For instance, let us consider the discharge cell parameters from Fig. 1. The coefficients A and B, particle mobilities, and diffusion coefficients for nitrogen can be found in Ref. [1]. We take $\gamma=0.02$ and obtain the breakdown voltage $U_b=885$ V. The right-hand side of Eq. (21) is 58 V, so that we assume $U_s=895$ V that results in $s=0.19$ and $j_0=10^{-5}$ A/cm^2. The corresponding set of parameters for the system (27) and (28) is given in Table I.

In general, the system dynamics is determined by two dimensionless ratios τ_u/τ_v and d_u/d_v, both quantities are of order unity in our example. Of course, either large or small ratios are also possible. In contrast to this, both u and v are always of order unity due to the normalization. The diffusion lengths d_u and d_v shall be smaller than the radial space scale R, nonlinearity is hence superior to diffusion. Typically, most of the physical space is occupied with homogeneous stationary solutions of Eqs. (27) and (28). The diffusion is only important in transition regions where spatial dependence of u or v is essential, e.g., in the case of ionization fronts.

Let us now systematically discuss solutions of the basic system (27) and (28).

A. Stationary states and ionization waves

The system (27) and (28) has two stationary homogeneous equilibrium solutions. The solution $(u=0,v=1)$ corresponds to vanishing current and peak overvoltage, it is referred to as the *overvoltage state*. The second solution $(u=1,v=0)$ describes a stationary *Townsend state*. As explained in the introduction, the system is assumed to be near the breakdown point when the supply voltage is suddenly increased to a value $U_s>U_b$. A corresponding initial condition for Eqs. (27) and (28) is $u=v=0$. An initial stage of the system evolution is described by the exact partial solution with $u\equiv0$ and

$$\tau_v\partial_t v=d_v^2\nabla_\perp^2 v+1-v,$$

which physically corresponds to the condenser charging. On the time scale τ_v the system reaches the overvoltage state. The latter, of course, is unstable. Assuming a small harmonic perturbation of the overvoltage state $u=0+\delta u, v=1+\delta v$ with the perturbation terms $\sim\exp(ikx+\Gamma t)$, we reduce Eqs. (27) and (28) to a dispersion relation for Γ. There are two real roots

$$\Gamma_1=\frac{1-(kd_u)^2}{\tau_u} \quad \text{and} \quad \Gamma_2=-\frac{1+(kd_v)^2}{\tau_v},$$

where the first root indicates an instability on the time scale τ_u. If $\tau_u<\tau_v$, the instability develops immediately after increase of the supply voltage and the overvoltage state is not really achieved. The instability corresponds to the breakdown and brings the system to the Townsend mode of operation. The latter is asymptotically stable. Indeed, we start from the Townsend state, add a small perturbation $u=1+\delta u, v=0+\delta v$ proportional to $\exp(ikx+\Gamma t)$, and arrive at the dispersion relation

$$\Gamma^2+\left(\frac{1}{\tau_v}+D_vk^2+D_uk^2\right)\Gamma+\frac{1}{\tau_u\tau_v}+\left(\frac{1}{\tau_v}+D_vk^2\right)D_uk^2=0,$$

where the diffusion coefficients

$$D_u=\frac{d_u^2}{\tau_u}=D_a \quad \text{and} \quad D_v=\frac{d_v^2}{\tau_v}=D_c.$$

One can check that $\mathrm{Re}\,\Gamma<0$ for all k. If in addition $\mathrm{Im}\,\Gamma\neq0$, the perturbation oscillates in space and time and can be interpreted as a decaying *ionization wave*. This happens if $\tau_u<4\tau_v$. The frequency $\omega_k=\mathrm{Im}\,\Gamma$ of such a wave is determined by the relation

$$\omega_k^2=\frac{1}{\tau_u\tau_v}\left(1-\frac{\tau_u}{4\tau_v}\right)+\frac{D_u-D_v}{2\tau_v}k^2, \tag{29}$$

where we took into account that the basic system (27) and (28) is valid only for the long-wave perturbations with $(kd_u)^2\ll1$ and $(kd_v)^2\ll1$. Note, that the group velocity of the ionization waves can be either parallel or opposite to the direction of the phase velocity depending on interplay of D_u and D_v.

We stress, that the above solutions correspond to a small perturbation of the stationary states, i.e., to linear waves. Essentially nonlinear solutions appear if we consider a dynamical transition from the overvoltage state to the Townsend state. The details of such a transition can be surprisingly different depending on the system parameters. These solutions are investigated below.

B. Uniform solutions

An important class of solutions of Eqs. (27) and (28) is generated if the discharge is uniform in space, i.e.,

$$\tau_u\dot{u}=uv, \tag{30}$$

$$\tau_v\dot{v}=1-u-v, \tag{31}$$

so that the basic system can be replaced by an equivalent second order equation

$$\tau_u\tau_v\ddot{v}+(\tau_u-\tau_v v)\dot{v}+v-v^2=0,$$

where the dot denotes derivation with respect to time. The equation describes a uniform transition from the overvoltage state to the Townsend state. A somewhat similar phenomenological system was originally suggested in Ref. [29].

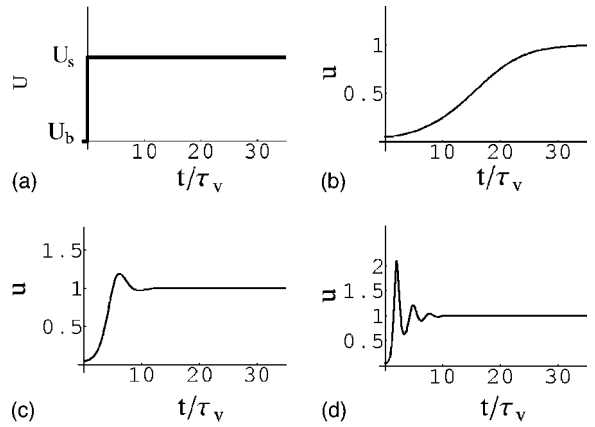

FIG. 2. Numerical results for temporal behavior of $u=j/j_0$ for uniform breakdown [Eqs. (30) and (31)]. Initial conditions are $u(0)=0.05$ and $v(0)=0.0$, i.e., the initial current fluctuation is 5% of the final value. (a) Applied voltage, arbitrary units; (b) $\tau_u/\tau_v=5$, no oscillations; (c) $\tau_u/\tau_v=1$, the current profile is nonmonotonic; (d) $\tau_u/\tau_v=0.2$, damping current oscillations.

For $\tau_u>4\tau_v$ the current increases monotonically. As above, if either the circuit capacity or resistivity are large enough and $\tau_u<4\tau_v$ the discharge current is subject to damped oscillations. If $\tau_u \ll \tau_v$ the corresponding Q-factor $Q=\sqrt{\tau_v/\tau_u}$ achieves large values and the oscillations have a well-defined frequency defined by Eq. (29) for $k=0$. However, the oscillations inevitably decay on the time scale τ_v. Physically they correspond to dumped transient oscillations to the steady state and should not be mixed with the subnormal discharge oscillations between Townsend and glow modes [25,30,31]. These undamped oscillations are caused by space-charge effect in the glow mode that is out of scope of this paper.

Figure 2 shows the electric current behavior for different values of τ_u/τ_v. It should be noted, that the uniform breakdown requires homogeneous initial perturbation (i.e., uniform distribution of seed electrons) that is highly unlikely. A more realistic picture corresponds to a small initial current fluctuation induced locally in space by a randomly localized group of seed electrons or by a local inhomogeneity of electrodes. It is then necessary to consider nonuniform solutions of Eqs. (27) and (28).

C. Fisher equation

The nonuniform breakdown, as a possible solution of Eqs. (27) and (28), occurs in the form of *ionization fronts*. Such a front is a transition wave between unstable and stable system states that propagates along the electrodes.

We start with a simple special case where the basic system (27) and (28) is reduced to the classical Fisher equation [32]. Let us assume that $\tau_v \ll \tau_u$ so that the time derivative in (28) can be ignored, i.e., the cathode current immediately follows the gas current. This happens, if the Maxwell time of the high ohmic barrier is not too large. We also assume that $d_v \ll d_u$, i.e., the current diffusion dominates the formal diffusion of the overvoltage. The latter is then directly determined from (28) $v=1-u$ and can be inserted into (27). We arrive at a closed adiabatic equation for the electric current

$$\tau_u \partial_t u = d_u^2 \nabla_\perp^2 u + u(1-u), \tag{32}$$

which is recognized as the Fisher equation. A lot of information is available for this equation [32], and we can easily draw various conclusions with respect to the breakdown under the above defined conditions. First of all, a small local current fluctuation leads to an exponential increase of the current. On the time scale τ_u the current density $j \sim j_0$ is nearby the original fluctuation. Further on, the instability develops in a nonlinear way, a monotonic ionization front propagates away from the initial fluctuation. Far away from the fluctuation point the front is practically one dimensional, stable, and has a special form $u=u(x-ct)$, where $u(-\infty)=1$ and $u(+\infty)=0$. If the initial fluctuation is well localized (see, e.g., Ref. [33]) the front velocity equals

$$c = \frac{2d_u}{\tau_u} = \frac{2\sqrt{D_e \tau_e}}{\tau_i} \sqrt{C_\gamma \alpha_b' (U_s - U_b)}, \tag{33}$$

where $\tau_e = d/(b_e E_b)$ is the electron travel time. For the nonlocalized initial conditions the front velocity exceeds c. The latter is proportional to the square root of the overvoltage, i.e., the front propagation differs from the familiar expansion of the current spot in the glow discharge mode [26], where the velocity is proportional to the overvoltage. During the ignition the radius of the current spot increases $\sim t$, the total current is $\sim t^2$. Finally the uniform state with $j=j_0$ is established on the whole electrodes area, except for plasma edges where boundary conditions affect final current distribution.

D. Ionization fronts

The preceding section explicitly describes front properties (e.g., form and stability) and provides an analytical expression for the lowest front velocity. This is possible because of the simple character of the Fisher equation. The general case of Eqs. (27) and (28) is more complicated, and we refer to the numerical solutions. Fortunately, our basic system is much more easy to solve than the original discharge Eqs. (6) and (7). In particular, because of the analytical expressions (9) and (10), we calculate in (x,y,t) space and obtain information in the whole three-dimensional (3D) physical space. In a typical run one can easily cover a macroscopical time interval (e.g., 10^3 ion travel times). In contrast to this, a direct numerical solution of the original 3D equations (6) and (7) for $t \gg \tau_i$ is a much more complicated problem.

Qualitatively, the behavior of the general solution is the same as for the Fisher case. An initial current perturbation changes to a stable ionization front. The latter propagates away from the initial perturbation and quickly changes to a quasi-one-dimensional front. If the initial fluctuation is well localized [33], front form and velocity are uniquely determined by $\tau_{u,v}$ and $d_{u,v}$, otherwise the velocity is larger and depends on fluctuation. The structure at the transition region of the front is more complicated than in the case of the Fisher equation. In addition to monotonic fronts, strongly oscillating fronts can be observed. An example of this case is shown in Fig. 3 where the system parameters from Table I were used.

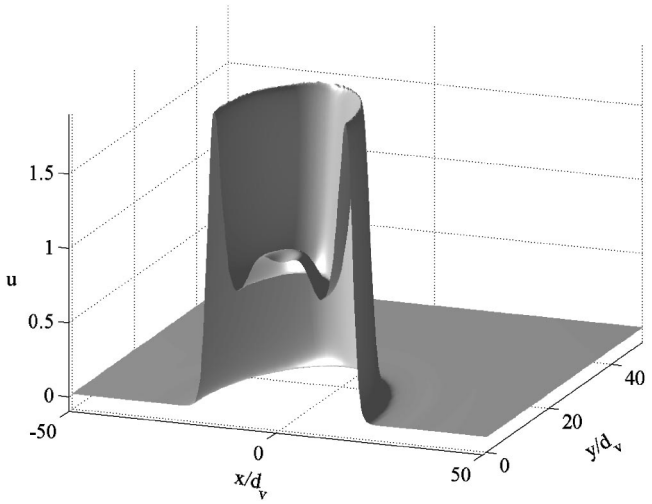

FIG. 3. Numerical results for spatial behavior of $u=j/j_0$ for ionization front [Eqs. (27) and (28)]. The Neumann boundary conditions and the system parameters from Table I were used. We started from $u=v=0$ and added a small fluctuation of u at the origin. The fluctuation changes to a front that spreads out with a constant velocity $\sim 3\times 10^4$ cm/s. The velocity depends on fluctuation but does not change with time or with refining of the numerics.

Four typical examples of front cross sections are shown in Fig. 4 for different parameters of the system. More complicated scenarios appear if there is more than one initial fluctuation. Several fronts are produced, they collide with each other and merge in the course of the collision processes. At the end, however, we always have only one front that transforms the system in the uniform Townsend state.

It is of interest to compare our results to those for metal electrodes. Considering the same discharge cell, except for metal electrodes and an equivalent external resistivity, one can derive the following system:

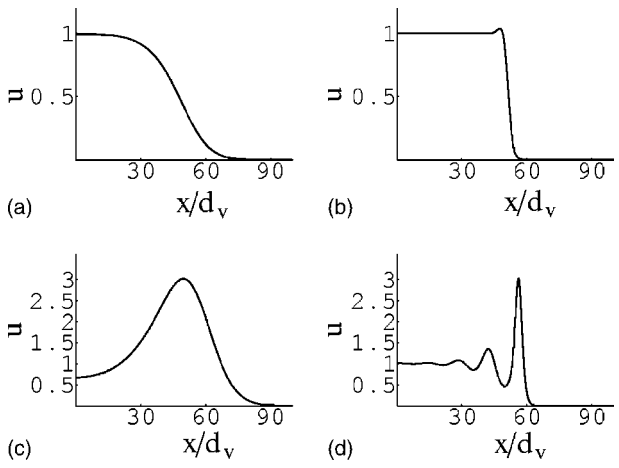

FIG. 4. Numerical results [Eqs. (27) and (28)] for the form of the ionization fronts for different system parameters. (a) $\tau_u/\tau_v=5$ and $d_u/d_v=4$, i.e., both time and space scales are determined by the gas; (b) $\tau_u/\tau_v=5$ and $d_u/d_v=0.25$, the cathode is adiabatic and diffusion in the gas is small; (c) $\tau_u/\tau_v=0.2$ and $d_u/d_v=4$, the discharge is adiabatic and formal diffusion in the cathode is small; (d) $\tau_u/\tau_v=0.2$ and $d_u/d_v=0.25$, both time and space scales are determined by the cathode.

$$\tau_u \partial_t u = d_u^2 \nabla_\perp^2 u + uv, \tag{34}$$

$$\tau_v d_t v = 1 - \langle u \rangle - v, \tag{35}$$

where the first equation is identical to Eq. (27), whereas the overvoltage is uniform $v=v(t)$ and subject to the ordinary differential equation. Here

$$\langle u \rangle = \frac{1}{S} \int \int u(x,y,t)dxdy$$

is the space-averaged value of the current density and S is the area of the electrodes. One immediate observation is that uniform solutions of Eqs. (34) and (35) are identical to those of Eqs. (27) and (28). Nonuniform solutions are however different owing to the absence of the overvoltage diffusion term and, more importantly, slow changes of $\langle u \rangle$. A seed current fluctuations develops in a current filament with a considerably larger amplitude as compared to those in Fig. 4. Neither fronts (i.e., well distinguished stationary states and a moving transition region between them) nor spatial oscillations are observed. The filament looks like a bell-shaped curve and that expands before the Townsend discharge state is achieved.

V. CONCLUSIONS

We investigated electric breakdown and transition to the Townsend discharge mode for a gaseous plane-parallel discharge cell. The discharge is stabilized by a *distributed* external resistor, e.g., a laterally extended high-ohmic cathode. Such a system exhibits a large variety of self-organized patterns and is a good candidate for a fundamental investigation of general properties of pattern formation in nonlinear spatially extended dissipative systems. In contrast to the good qualitative understanding of experimentally observed patterns, the system with the high-ohmic cathode was never investigated quantitatively on the basis of gas-discharge specific transport equations. In a first step we developed such a description on the base of classical *drift-diffusion* discharge model in the Townsend mode of operation.

The key problem is that the experimental phenomena are observed on a macroscopic time scale (of the order of 10^{-3} s or longer), whereas the drift-diffusion approximation is on a microscopic time scale (e.g., the electron travel time which is $\simeq 4\times 10^{-9}$ s for the system in Fig. 1). A direct numerical solution of the full 3D drift-diffusion equations on macroscopical times is practically impossible and a reduction of the drift-diffusion model is desirable. Such a reduction is developed in the present paper using the fact that the axial dimension of the discharge cell in question is small as compared to the radial dimension. Two-scale approach allows then to separate off the axial and radial effects. The reduction is possible if the source voltage exceeds the breakdown voltage to only a small extent [Eq. (21)] that ensures the slow evolution of the system.

The drift-diffusion equations are simplified to a two-component *reaction-diffusion* system, that incorporates only radial coordinates and slow time evolution. All numerical

coefficients in our system can be quantitatively calculated, that is, our predictions can be compared with experimental data. For instance, the solution displayed in Fig. 3 should be observed for the discharge cell parameters from Fig. 1. The derived set of Eqs. (27) and (28) is much better suited for analytical and numerical investigations than the full drift-diffusion set of equations. In particular, in Eqs. (27) and (28) the solution in full 3D space must be implemented numerically only for two space coordinates because the axial dependence is taken into account analytically.

The most important nontrivial solutions of Eqs. (27) and (28) are those for nonlinear ionization fronts, which propagate along the discharge plane away from the point of ignition. In some special cases the lowest front velocity can be calculated analytically [Eq. (33)], in general the velocity depends on triggering fluctuation and one must find a numerical solution. The form of the ionization front can be either monotonic or oscillating (Fig. 4). Such an oscillating behavior is specific for the distributed external resistor and does not occur for ordinary metal electrodes.

In closing, the present approach is a first step in the quantitative description of pattern formation phenomena in planar dc gas-discharge systems as cited above. In a second step the treatment must be extended from the Townsend mode of operation to the glow discharge mode where the patterns are actually observed. Also in this case a relatively simple reaction diffusion system, but with a cubic nonlinearity, can be derived. Corresponding work is in progress.

ACKNOWLEDGMENTS

The authors gratefully acknowledge useful discussions with M. S. Benilov, Y. P. Raizer, and L. D. Tsendin. The authors also thank Deutsche Forschungsgemeinschaft for financial support.

[1] Yu. P. Raizer, *Gas Discharge Physics* (Springer-Verlag, Berlin, 1991).
[2] H.-G. Purwins, G. Klempt, and J. Berkemeier, Festkoerperprobleme **27**, 27 (1987).
[3] H.-G. Purwins, C. Radehaus, and J. Berkemeier, Z. Naturforsch., A: Phys. Sci. **43**, 17 (1988).
[4] H. Willebrand, C. Radehaus, F.-J. Niedernostheide, R. Dohmen, and H.-G. Purwins, Phys. Lett. A **149**, 131 (1990).
[5] E. L. Gurevich, A. W. Liehr, Sh. Amiranashvili, and H.-G. Purwins, Phys. Rev. E **69**, 036211 (2004).
[6] Y. A. Astrov, E. Ammelt, S. Teperick, and H.-G. Purwins, Phys. Lett. A **211**, 184 (1996).
[7] Y. A. Astrov, E. Ammelt, and H.-G. Purwins, Phys. Rev. Lett. **78**, 3129 (1997).
[8] E. Ammelt, Y. A. Astrov, and H.-G. Purwins, Phys. Rev. E **55**, 6731 (1997).
[9] Y. A. Astrov, I. Muller, E. Ammelt, and H.-G. Purwins, Phys. Rev. Lett. **80**, 5341 (1998).
[10] E. Ammelt, Y. A. Astrov, and H.-G. Purwins, Phys. Rev. E **58**, 7109 (1998).
[11] C. Strumpel, Y. A. Astrov, E. Ammelt, and H.-G. Purwins, Phys. Rev. E **61**, 4899 (2000).
[12] C. Strumpel, Y. A. Astrov, and H.-G. Purwins, Phys. Rev. E **62**, 4889 (2000).
[13] C. Strumpel, H.-G. Purwins, and Y. A. Astrov, Phys. Rev. E **63**, 026409 (2001).
[14] Y. A. Astrov and H.-G. Purwins, Phys. Lett. A **283**, 349 (2001).
[15] E. L. Gurevich, A. S. Moskalenko, A. L. Zanin, Y. A. Astrov, and H.-G. Purwins, Phys. Lett. A **307**, 299 (2003).
[16] M. C. Cross and P. Hohenberg, Rev. Mod. Phys. **65**, 851 (1993).
[17] M. S. Benilov, Phys. Rev. A **45**, 5901 (1992).
[18] R. Sh. Islamov, Phys. Rev. E **64**, 046405 (2001).
[19] E. L. Gurevich, Yu. A. Astrov, and H.-G. Purwins, J. Phys. D **38**, 468 (2005).
[20] V. A. Lisovsky, S. D. Yakovin, and V. D. Yegorenkov, J. Phys. D **33**, 2722 (2000).
[21] L. M. Portsel, Yu. A. Astrov, I. Reimann, and H.-G. Purwins, J. Appl. Phys. **81**, 1077 (1997).
[22] Yu. P. Raizer and S. T. Surzhikov, High Temp. **28**, 324 (1990).
[23] V. A. Schweigert, Tech. Phys. Lett. **19**, 659 (1993).
[24] V. A. Schweigert, Tech. Phys. **38**, 384 (1993).
[25] V. I. Kolobov and A. Fiala, Phys. Rev. E **50**, 3018 (1994).
[26] Yu. P. Raizer and S. T. Surzhikov, High Temp. **31**, 19 (1993).
[27] I. D. Kaganovich, M. A. Fodotov, and L. D. Tsendin, Tech. Phys. **39**, 241 (1994).
[28] A. A. Kudryavtsev and L. D. Tsendin, Tech. Phys. Lett. **28**, 1036 (2002).
[29] Yu. A. Astrov, A. F. Ioffe Physico-Technical Institute Report No. 1255, 1988, in Russian.
[30] R. R. Arslanbekov and V. I. Kolobov, J. Phys. D **36**, 2986 (2003).
[31] D. D. Sijacic, U. Ebert, and I. Rafatov, Phys. Rev. E **70**, 056220 (2004).
[32] J. D. Murray, *Mathematical Biology*, Biomathematics Vol. 19 (Springer, Berlin, 1989).
[33] W. van Saarloos, Phys. Rep. **386**, 29 (2003).